Draft version September 17, 2018
Typeset using LaTeX **twocolumn** style in AASTeX62

Controlling the rotational constraint in stratified, compressible convection

Evan H. Anders,[1,2] Cathryn M. Manduca,[2] and Benjamin P. Brown[1,2]

[1] *Dept. Astrophysical & Planetary Sciences, University of Colorado – Boulder, Boulder, CO 80309, USA*
[2] *Laboratory for Atmospheric and Space Physics, Boulder, CO 80303, USA*

(Received September 17, 2018; Revised September 17, 2018; Accepted September 17, 2018)

Submitted to ApJ

ABSTRACT

Keywords: convection — happy caterpillars

1. INTRODUCTION

Convection under the influence of rotation has been studied in great detail in recent decades. In the incompressible boussinesq case, numerous authors have studied rotating convection in both laboratory and numerical settings. The behavior of the heat transport in these systems has been the focus of many of these studies, particularly the difference of behavior of heat transport in rotationally-constrained and unconstrained regimes (King et al. 2009; Zhong et al. 2009; Stevens et al. 2009; Julien et al. 2012). Studies of both laboratory (cite, cite) and numerical (cite, cite) experiments coincide well in these regimes.

More complicated experiments of rotational convection are often conducted using numerical tools in spherical geometries. Often these studies aim to gain insight into the solar dynamo (Glatzmaier & Gilman 1982; Busse 2002; Brown et al. 2008, 2010, 2011; Augustson et al. 2012; Guerrero et al. 2013; Käpylä et al. 2014). Numerous interesting phenomenological discoveries have been made in such studies, but they often employ very different degrees of rotational constraint, but their basic system behavior often differs significantly from the sun. For example, dynamo simulations often produce antisolar differential rotation profiles at nominally solar values of rotational constraint.

In recent years, helioseismic imaging of flows in the Sun have suggested that power in large-scale convective motions is much lower than convective simulations and mixing length theory predict (Hanasoge et al. 2012; Greer et al. 2015). This suggests that either convection is not driven deep in the solar convection zone or its motions are masked before they reach the surface by some process. A number of possible mechanisms have been suggested as culprits for this behavior, including entropy rain (Brandenburg 2016). One other possibility is that the interior convection zone is rotationally constrained, and that this behavior is reducing low wavenumber power at the surface. The recent work of Featherstone & Hindman (2016) suggests that this is a strong possibility, and the observations of Greer et al. (2016) suggest that flows in the deep solar convection zone are rotationally constrained. The degree of rotational constraint under which convective flows occur can greatly change the character of the resultant situation, and so in the case of astrophysical contexts (solar studies such as those mentioned above and also planetary studies such as e.g., Soderlund et al. (2015)), it is important to study convection in the same rotational regime as the astrophysical object of interest in order to meaningfully understand results.

One difficulty in studying rotational convection is that it is often unclear from input parameters whether or not the resulting convective state will be rotationally constrained. In Anders & Brown (2017) (hereafter AB17), we studied non-rotating, hydrodynamic, compressible convection. We showed how the evolved Reynolds number, Peclet number (Re and Pe, two measures of turbulence in the evolved state), and Mach number (Ma, the ratio of flow speed to the local sound speed) of the convective solution can be specified through a properly constructed reference atmosphere. Upon the inclusion of rotation, a fourth dynamical measure of the solution becomes meaningful: the Rossby number (Ro, the ratio of advective dynamics to rotational constraint). Low Ro

Corresponding author: Evan H. Anders
evan.anders@colorado.edu

flows are rotationally constrained, while high Ro flows are not. While the literature contains a wealth of information regarding how the magnitude of rotation affects the heat transport characteristics of convection, we find no work which simply links the rotational constraint of evolved solutions with input parameters.

In this work, we extend the study of AB17 to rotationally-influenced, f-plane polytropic atmospheres, as have been previously studied by e.g., Brummell et al. (1996, 1998); Calkins et al. (2015). Our goal is to determine how the input parameters which we studied previously couple with a new input parameter, the Taylor number (Ta, Julien et al. (1996)), which sets the magnitude of the rotational vector. In section 2, we describe our atmosphere, numerical experiment, and paths through parameter space. In section 3, we present the results of our experiments and we offer concluding remarks.

2. EXPERIMENT

We study fully compressible, stratified convection as we previously did in Anders & Brown (2017), with the inclusion of rotation. We study an ideal gas whose equation of state is $P = R\rho T$ and with an adiabatic index $\gamma = 5/3$. We nondimensionalize the atmosphere such that $R = 1$ and $P = \rho = T = 1$ at the top of the domain. The initial stratification is polytropic, such that

$$\begin{aligned} \rho_0(z) &= (1 + L_z - z)^m, \\ T_0(z) &= (1 + L_z - z), \end{aligned} \tag{1}$$

where m is the polytropic index, z increases upwards in the range $z = [0, L_z]$, and $L_z \equiv e^{n_\rho/m} - 1$ is the depth of the atmosphere, where n_ρ specifies the number of density scale heights that the atmosphere spans. We specify the instability of the atmosphere through the superadiabatic excess, $\epsilon = m - m_{ad}$, where $m_{ad} = (\gamma - 1)^{-1}$ is the adiabatic polytropic index, and ϵ controls the Mach number of the flows (Anders & Brown 2017). The domain is a 3D cartesian box whose horizontal extent is in the range $x, y = [0, AL_z]$, where A is the aspect ratio of the domain. As has been studied previously by e.g., Julien et al. (1996); Brummell et al. (1996), we study a domain in which the gravity and rotational vector are antiparallel, $\boldsymbol{g} = -g\hat{z}$, and $\boldsymbol{\Omega} = \Omega\hat{z}$.

We evolve the velocity ($\boldsymbol{u}$), temperature, and log density according to the Fully Compressible Navier-Stokes equations,

$$\frac{\partial \ln\rho}{\partial t} + \nabla\cdot\boldsymbol{u} = -\boldsymbol{u}\cdot\nabla\ln\rho, \tag{2}$$

$$\begin{aligned} \frac{\partial \boldsymbol{u}}{\partial t} + 2\boldsymbol{\Omega}\times\boldsymbol{u} + \nabla T - \nu\nabla\cdot\bar{\bar{\boldsymbol{\sigma}}} - \bar{\bar{\boldsymbol{\sigma}}}\cdot\nabla\nu = \\ -\boldsymbol{u}\cdot\nabla\boldsymbol{u} - T\nabla\ln\rho + \boldsymbol{g} + \nu\bar{\bar{\boldsymbol{\sigma}}}\cdot\nabla\ln\rho, \end{aligned} \tag{3}$$

$$\begin{aligned} \frac{\partial T}{\partial t} - \frac{1}{c_V}\left(\chi\,\nabla^2 T + \nabla T\cdot\nabla\chi\right) = \\ -\boldsymbol{u}\cdot\nabla T - (\gamma-1)T\nabla\cdot\boldsymbol{u} \\ + \frac{1}{c_V}\left(\chi\nabla T\cdot\nabla\ln\rho + \nu\left[\bar{\bar{\boldsymbol{\sigma}}}\cdot\nabla\right]\cdot\boldsymbol{u}\right), \end{aligned} \tag{4}$$

with the viscous stress tensor given by

$$\sigma_{ij} \equiv \left(\frac{\partial u_i}{\partial x_j} + \frac{\partial u_j}{\partial x_i} - \frac{2}{3}\delta_{ij}\nabla\cdot\boldsymbol{u}\right). \tag{5}$$

The kinematic viscosity, ν, thermal diffusivity, χ, and strength of rotation Ω are set at the top of the domain by the Rayleigh number (Ra), Prandtl number (Pr), and Taylor number (Ta),

$$\mathrm{Ra} = \frac{gL_z^3\Delta S/c_P}{\nu\chi},\quad \mathrm{Pr} = \frac{\nu}{\chi},\quad \mathrm{Ta} = \left(\frac{2\Omega L_z^2}{\nu}\right)^2, \tag{6}$$

where $\Delta S = \epsilon n_\rho/m$ is the specific entropy difference between $z = 0$ and $z = L_z$, and the specific heat at constant pressure is c_P.

As Ta increases, the critical value of Ra at which convection onsets, $\mathrm{Ra_{crit}}$, also increases. The linked nature of these crucial control parameters makes it difficult to predict the regime of the evolved fluid flows for a given set of input parameters. In this work, we will explore commonly-chosen paths through Ra-Ta space, as well as an additional experimentally-determined path. These three paths are defined as

$$\mathrm{Ra} = \begin{cases} (1+\sigma)\mathrm{Ra_{crit}}(\mathrm{Ta}), \\ \mathrm{Co}^2\mathrm{Pr}\ \mathrm{Ta}, \\ \mathcal{C}^2\mathrm{Pr}\ \mathrm{Ta}^{3/4}. \end{cases} \tag{7}$$

Here, $(1 + \sigma)$ is the supercriticality, and the first path through this parameter space is at constant supercriticality and Co is the classic "Convective Rossby number," which has been used frequently over the past two decades, and is intended to predict the rotational constraint of the evolved solution (Julien et al. 1996; Brummell et al. 1996). Paths through parameter space at constant $\mathcal{C}$, which we call the Predictive Rossby Number, are along countours of $\mathrm{Ta}^{3/4}$ are a new path through parameter space that we explore in this work. An example

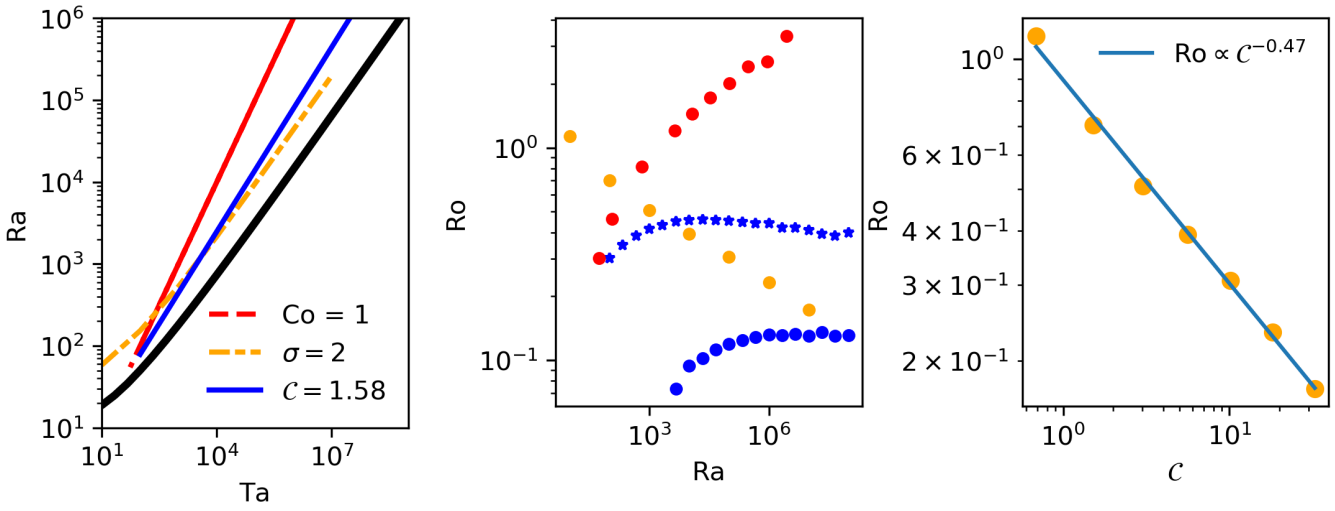

Figure 1. (a) The critical Rayleigh number, as a function of the Taylor number, is plotted as a solid black line. Paths of constant Convective Rossby Number (red dashed line), constant supercriticality (orange dashed line), and $\mathcal{C}$ (blue solid line) are shown through parameter space. (b) Evolved Rossby number is plotted vs. Taylor number along multiple constant $\mathcal{C}$ paths, such as the solid blue line in (a). After a sharp increase at low Ta, the evolved Rossby number flattens out and stays nearly constant across orders of magnitude of Ta.

of each of these paths can be seen in Fig. 1a. Our goal is to find a path along which the Rossby number,

$$\mathrm{Ro} = \frac{|\nabla \times \boldsymbol{u}|}{2\Omega}, \tag{8}$$

and thus the rotational constraint of the flows, is constant.

3. RESULTS & DISCUSSION

In Fig. 1a, we display the value of the critical Rayleigh number ($\mathrm{Ra_{crit}}$) as a function of the Taylor number (Ta). We found these critical values through the use of a linear instability analysis. We plot sample paths through this parameter space at $\sigma = 1$, $\mathrm{Co} = 1$, and $\mathcal{C} = 0.957$, as defined in Eqn. 7. In Fig. 1b, we show that along paths of constant σ, the Rossby number, as defined in Eqn. 8, decreases weakly as a function of Ra and Ta. Along paths of constant Co, Ro increases sharply with increasing Ra and Ta. However, along paths of constant $\mathcal{C}$, after an increase at low Ra, the evolved value of Ro levels off and stays roughly constant as a function of Ra. By interpolating between the slopes of constant σ and constant Co lines, we arrived at the scaling of $\mathrm{Ra} \propto \mathrm{Ta}^{3/4}$ along constant $\mathcal{C}$ lines, and holding $\mathcal{C}$ constant seems to predict Ro relatively well from our experimental trials here. In Fig. 1c, we show how the Predictive Rossby Number, $\mathcal{C}$, relates to the evolved Rossby number for a series of runs which are all at the same supercriticality.

We define the Nusselt number (Nu) as we did previously in AB17,

$$\mathrm{Nu} \equiv \frac{\langle F_{\mathrm{conv,z}} + F_{\mathrm{cond,z}} - F_{\mathrm{A}} \rangle}{\langle F_{\mathrm{cond,z}} - F_{\mathrm{A}} \rangle}, \tag{9}$$

where $F_{\mathrm{conv,z}}$ is the vertical convective flux, $F_{\mathrm{cond,z}}$ is the vertical conductive flux, and F_{A} is the adiabatic conductive flux. We refer the reader to AB17 for a more thorough definition of these fluxes. In Fig. 2a, we show the scaling of the Nusselt number as a function of Ra at fixed $\mathcal{C}$. We find that when $\mathcal{C}$ is held constant and Ra is increased, we find a scaling of $\mathrm{Nu} \propto \mathrm{Ra}^{2/7}$ [note: insert true scaling], reminiscent of classical scaling laws in non-rotating theory as Ra increases. Furthermore, in Fig. 2b, we plot the RMS Reynold's number ($\mathrm{Re} = |u|L_z/\nu$) as a function of Ra, and find that $\mathrm{Re} \propto \mathrm{Ra}^{1/2}$, which is reminiscent of how the Reynold's number scales with increasing Ra in non-rotating convection.

In Fig. 3, we show sample snapshots of the convective flows in our domain. I'll need to talk about them once I get there.

In Fig. 4, we show time- and horizontally-averaged profiles of the rossby number and the entropy gradient. As Ra increases at a constant value of $\mathcal{C}$, both the entropy and rotational boundary layers shrink. We measure the upper boundary layer thicknesses of both profiles. We measure the boundary layer thickness of the Rossby number as the distance from the upper boundary to the point at which Ro is maximized. We measure the boundary layer thickness of the entropy profile by fitting a line to the upper 10 points in the domain, and assuming that the boundary layer extends to the point at which that line crosses through zero. We plot $\delta_S/\delta_{\mathrm{Ro}}$ as a function of Ra for our $\mathcal{C}$ paths in Fig. 4b. We find that the ratio of these boundary layers is relatively constant as a fucntion of Ra, which implies that the rota-

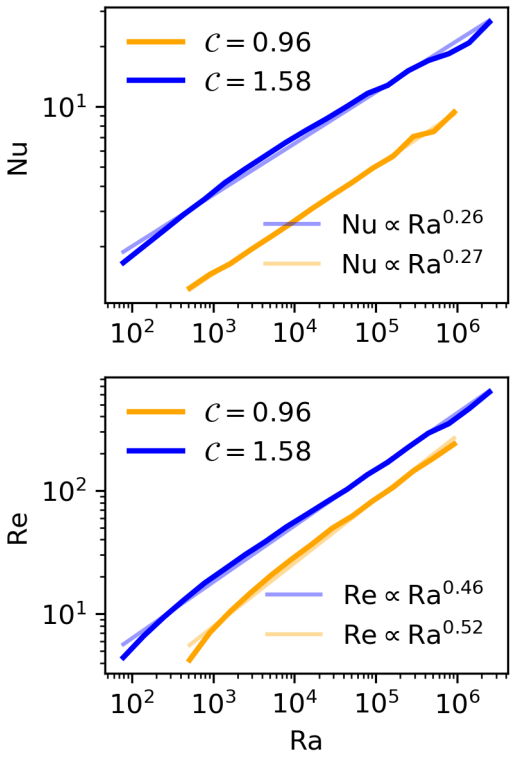

Figure 2. (a) Evolved Nusselt number vs. Rayleigh number / Ra_crit along constant $\mathcal{C}$ paths. A classic scaling law of $Nu \propto Ra^{2/7}$ is observed. (b) Evolved Reynolds number vs. Rayleigh number / Ra_crit along constant $\mathcal{C}$ paths. A classic scaling law of $Re \propto Ra^{1/2}$ is observed. These laws are reminiscent of standard scaling laws of Re and Nu in non-rotational convection (SOURCES SOURCES SOURCES). This suggests that at fixed Rossby number on a constant $\mathcal{C}$ path (Fig. 1), varying the Rayleigh number affects the evolved dynamics in a manner similar to a nonrotating fluid.

Figure 3. Here's some pretty plots, we'll figure out what we plot later.

Figure 4. (a) Horizontally-averaged profiles of the Rossby number are shown vs. z for a constant $\mathcal{C}$ = X. (b) Horizontally-averaged profiles of the entropy gradient are shown vs. z for a constant $\mathcal{C}$ = X. (c) Vorticity boundary layer thickness normalized by entropy boundary layer thickness as a function of Ta/Ta_crit for multiple $\mathcal{C}$ paths. When this measure is $\gg 1$, we expect the flows to be buoyancy dominated, when it is $\ll 1$, we expect the flows to be rotationally dominated, and when it is ~ 1, we anticipate that both effects are very important.

tional constraint across Ra is roughly constant. [NOTE: NEED TO TALK ABOUT MAGNITUDE OF RO IN BOUNDARY LAYER]

4. DISCUSSION

In this letter, we studied rotating, stratified, compressible convection at low Mach number. We studied traditional paths through Ra-Ta space, as well as a new path, in which the Predictive Rossby number $\mathcal{C}$ is held constant, and $\mathrm{Ra} = \mathcal{C}\mathrm{Ta}^{3/4}$. Along these paths, we find that the evolved rotational constraint, as measured by the Rossby number (Ro), is roughly constant as Ra increases. Furthermore, the heat transport, measured by the Nusselt number (Nu), and the level of turbulence, as measured by the Reynolds number (Re), vary according to traditional scaling laws as Ra increases. Together, these phenomena suggest that experimenters in stratified convection can specify the degree of rotational constraint in their evolved solutions by choosing $\mathcal{C}$, and then increase Ra in a manner analogous to unrotating convection (e.g., AB17) to increase the efficiency and turbulent nature of the convective dynamics in question.

4.1. *acknowledgements*

EHA acknowledges the support of the University of Colorado's George Ellery Hale Graduate Student Fellowship. This work was additionally supported by NASA LWS grant number NNX16AC92G. Computations were conducted with support by the NASA High End Computing (HEC) Program through the NASA Advanced Supercomputing (NAS) Division at Ames Research Center on Pleiades with allocations GID s1647. We thank Jeff Oishi for many useful discussions.

REFERENCES

Anders, E. H., & Brown, B. P. 2017, Physical Review Fluids, 2, 083501

Augustson, K. C., Brown, B. P., Brun, A. S., Miesch, M. S., & Toomre, J. 2012, ApJ, 756, 169

Brandenburg, A. 2016, ApJ, 832, 6

Brown, B. P., Browning, M. K., Brun, A. S., Miesch, M. S., & Toomre, J. 2008, ApJ, 689, 1354

—. 2010, ApJ, 711, 424

Brown, B. P., Miesch, M. S., Browning, M. K., Brun, A. S., & Toomre, J. 2011, ApJ, 731, 69

Brummell, N. H., Hurlburt, N. E., & Toomre, J. 1996, ApJ, 473, 494

—. 1998, ApJ, 493, 955

Busse, F. H. 2002, Physics of Fluids, 14, 1301

Calkins, M. A., Julien, K., & Marti, P. 2015, Geophysical and Astrophysical Fluid Dynamics, 109, 422

Featherstone, N. A., & Hindman, B. W. 2016, ApJ, 830, L15

Glatzmaier, G. A., & Gilman, P. A. 1982, ApJ, 256, 316

Greer, B. J., Hindman, B. W., Featherstone, N. A., & Toomre, J. 2015, ApJL, 803, L17

Greer, B. J., Hindman, B. W., & Toomre, J. 2016, ApJ, 824, 4

Guerrero, G., Smolarkiewicz, P. K., Kosovichev, A. G., & Mansour, N. N. 2013, ApJ, 779, 176

Hanasoge, S. M., Duvall, T. L., & Sreenivasan, K. R. 2012, Proceedings of the National Academy of Science, 109, 11928

Julien, K., Knobloch, E., Rubio, A. M., & Vasil, G. M. 2012, Physical Review Letters, 109, 254503

Julien, K., Legg, S., McWilliams, J., & Werne, J. 1996, Journal of Fluid Mechanics, 322, 243

Käpylä, P. J., Käpylä, M. J., & Brandenburg, A. 2014, A&A, 570, A43

King, E. M., Stellmach, S., Noir, J., Hansen, U., & Aurnou, J. M. 2009, Nature, 457, 301

Soderlund, K. M., Sheyko, A., King, E. M., & Aurnou, J. M. 2015, Progress in Earth and Planetary Science, 2, 24

Stevens, R. J. A. M., Zhong, J.-Q., Clercx, H. J. H., Ahlers, G., & Lohse, D. 2009, PhRvL, 103, 024503

Zhong, J.-Q., Stevens, R. J. A. M., Clercx, H. J. H., et al. 2009, Physical Review Letters, 102, 044502